

BSc Thesis Applied Mathematics
and Applied Physics

**Avalanche nucleation by
impacting an inclined plane of
granular material with a
particle**

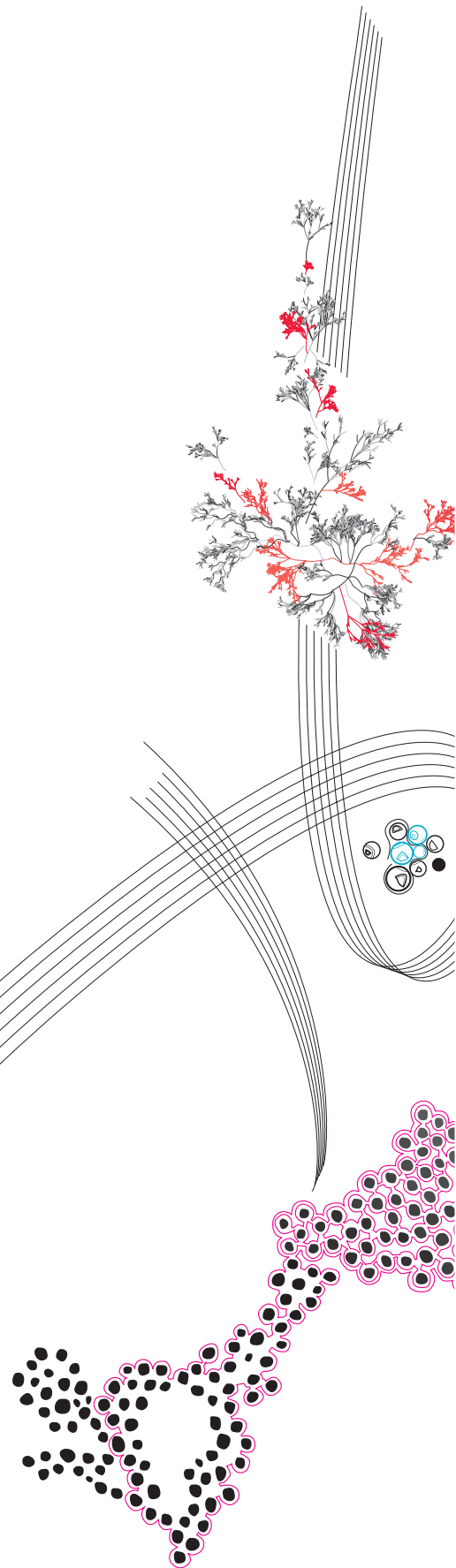
Anne Meulenkamp

Supervisor: B. Geurts, D. van der Meer

January, 2021

Department of Applied Mathematics
Faculty of Electrical Engineering,
Mathematics and Computer Science

Department of Applied Physics
Faculty of Science and Technology



Preface

I want to thank Bernard Geurts and Devaraj van der Meer for their support and enthusiasm for this project. Without their input and suggestions, this project would not have gotten started. I would like to thank Thomas Weinhardt for putting time and effort into helping me with MercuryDPM, both for installation purposes and the code. Lastly, I would like to thank Tjeerd Heering for his technical support in explaining Linux and C++, which greatly shortened the time it took before the research could begin.

Avalanche nucleation by impacting an inclined plane of granular material with a particle

Anne Meulenkamp*

January, 2021

Abstract

Early detection of unstable slopes where an avalanche is likely to occur in the near future is critical for timely evacuation of people nearby. This necessitates a method to determine how unstable a slope is. This paper seeks to determine the relation between the slope angle and the kinetic energy needed to start an avalanche. MercuryDPM is used to simulate an inclined plane of glass beads upon which an additional bead is dropped from varying heights. The occurrence of an avalanche was based on a minimum kinetic energy present in the system at some time after impact. It was determined that there is a linear correlation between the slope angle and drop height needed to initiate an avalanche. There was a notable topographical influence on the occurrence of an avalanche at certain angles.

Keywords: avalanche, granular material, inclined plane, nucleation, angle of repose

1 Introduction

Every year, all around the world, avalanches occur. These range from snow avalanches and rock avalanches to mud slides. Some of these avalanches destroy villages, causing the deaths of the people living there. There are many ways to reduce these deaths, by predicting the direction of an avalanche, the size of avalanche, and the speed of an avalanche. All of these can help decide which areas need to be evacuated when. Since avalanches travel fast, once an avalanche has started it may already be too late for any evacuation. In order to prevent this situation, it is necessary to know beforehand when a slope is close to collapsing and causing an avalanche. With this knowledge, it would then be possible to evacuate people ahead of a critical event and instead choose to trigger an avalanche when no one is around.

There has been a significant amount of research in the past 40 years on the flow of avalanches of granular material. Much of this research uses the principles of continuum fluid dynamics: Navier-Stokes, conservation of mass and momentum, and shear stress. Different types and parts of avalanches show different behaviour. In fig. 1 it can be seen that there are three different flow regimes in an avalanche. The top layer where the beads bounce in all directions is called the gaseous layer, since the movement of the beads resembles that of gases as the average distance

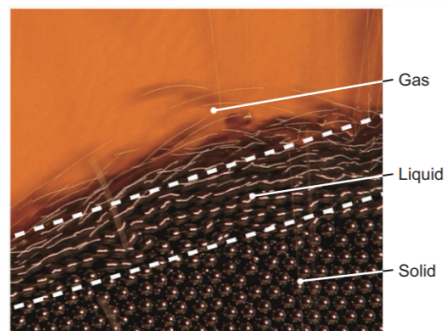


FIGURE 1: An illustration of the solid, liquid and gas flow regimes obtained by pouring steel beads on a pile [3].

*Email: a.r.meulenkamp@student.utwente.nl

between two particles is greater than their diameters. In the middle layer the entire layer flows down the slope, closely resembling a liquid with an average distance around a diameter, and in the bottom layer the beads either do not move or move very slowly, acting like solid material where the particles are touching each other.

Most models for granular avalanches are based on the Savage-Hutter model [6], which uses a shallow water approximation for the flowing layer of debris. Most of this research focuses on the shape, size and propagation speed of avalanches once they have come into existence, not on the stability of the slope. For particles on an inclined plane, pile or rotating drum it has already been shown that the free surface must be tilted above the angle of repose θ_{start} for an avalanche to occur naturally [3]. The avalanche would then continue to flow until a second critical angle θ_{stop} is reached where the material will slow down until it stops flowing. In reality this happens because the slope in the valley next to the mountain is less steep than on the mountain. The value of θ_{start} and the difference between θ_{start} and θ_{stop} are believed to depend on various parameters, among which the number of layers of free particles on the inclined plane [5]. In literature, some studies look at slopes under the angle of repose, meaning that the slope is stable [2]. However, this research does not address when or how an avalanche is triggered, but is concerned with the comparison between a triggered avalanche and a naturally occurring avalanche [2].

Prior to an avalanche there would be a slope of particles lying still, thus being in the solid regime. At some point after a fraction of the particles would start moving down the slope, the other two regimes could come into play. Hence, at the start of an avalanche it can be assumed that the particles on the slope can be reasonably modelled as individual solid particles, with the forces of friction and gravity still balanced to prevent a natural avalanche. In this paper, we investigate how much kinetic energy is needed to cause an avalanche on an inclined plane of spherical glass particles by dropping a particle on the slope. Here, we speak of an avalanche in case a minimum kinetic energy is reached at some time after the impact. We look at the relation between the necessary kinetic energy and the angle of the inclined plane to set off such an avalanche, as well as the influence of the topography of the slope on the nucleation of an avalanche. This is done using detailed granular simulations based on MercuryDPM, which is a collision-based particle simulator. This research focuses on spherical glass particles, leaving the influence of different shapes, sizes, and materials yet to be investigated. The organization of this paper is as follows. In section 2 the theory applied in MercuryDPM as well as the choices made in terms of particle type, size, number etc. are addressed. Subsequently, the results for natural and triggered avalanches for the first slope are shown in section 3.1. This is followed by section 3.2 in which we discuss the differences and similarities in the results obtained from 3 different slopes.

2 Methods

2.1 MercuryDPM

MercuryDPM is an open source project for discrete particle simulations written in C++. It simulates the movement of particles by applying forces and torques that stem from external forces such as gravity or from contact forces such as elastic, plastic, viscous and frictional forces [8].

2.1.1 Physical principles

MercuryDPM uses species to denote all variables concerned with the particle type. The species used in this paper is LinearViscoelasticFrictionSpecies. This simply means that elasticity and friction is included, but adhesion is excluded. In this case, no deformation due to twisting is present, thus torsion is set to 0. The code uses both forces and torques to determine the motion of the particles according to Newton's Laws. For particle i this results in

$$m_i \ddot{\vec{r}}_i = \vec{F}_i \quad (1)$$

$$I_i \dot{\vec{\omega}}_i = \vec{\tau}_i \quad (2)$$

with \vec{r}_i as the position vector, m_i as the mass, $\vec{\omega}_i$ as the angular velocity and I_i as the inertia. The resultant force (\vec{F}_i) and the resultant torque ($\vec{\tau}_i$) are given by

$$\vec{F}_i = \vec{F}_i^{ext} + \sum_{j=1}^N \vec{F}_{ij}^{int} \quad (3)$$

$$\vec{\tau}_i = \sum_{j=1}^N \vec{\tau}_{ij} + (\vec{c}_{ij} - \vec{r}_i) \times (\vec{F}_{ij}^{int}) \quad (4)$$

where the summations run over all particles j that are in contact with particle i , \vec{F}_i^{ext} are the external forces, \vec{F}_{ij}^{int} are the internal forces (i.e. forces between particles), $\vec{\tau}_{ij}$ is the torque due to rolling friction, and \vec{c}_{ij} is the location of the contact point between particles i and j . The only external force is the force of gravity, and the internal forces are due to sliding friction and elasticity. These forces and torques can be found in appendix A. The coefficients used to compute these forces and torques are placed in table 1.

TABLE 1: The values for the various variables as defined in MercuryDPM due to the particle material in SI-units. Variables denoted with a star are based on experimental data [8], the others are derived in appendix A.1

| | | | |
|------------------------------|---------------|------------|---|
| density | ρ | 2500 | * |
| stiffness | k | 258.41 | |
| dissipation | γ | 0.0079742 | |
| sliding stiffness | k_{sl} | 78.866 | |
| sliding dissipation | γ_{sl} | 0.0614092 | |
| sliding friction coefficient | μ_{sl} | 0.08 | |
| rolling stiffness | k_{ro} | 103.364 | |
| rolling dissipation | γ_{ro} | 0.00318968 | |
| rolling friction coefficient | μ_{ro} | 0.02 | |
| mass | m | 0.001309 | |
| radius | a | 0.005 | |
| collision time | t_c | 0.005 | * |
| normal restitution | ϵ | 0.97 | * |
| tangential restitution | β | 0.44 | * |

2.1.2 Discretization scheme

Since MercuryDPM is a discrete particle simulator, it naturally uses a discretization scheme. MercuryDPM uses a Velocity Verlet integrator [10] which is a variation of the leapfrog scheme [9]. The integrator has a global error of order 2 in time for both position and velocity; the local position error is 4th order accurate and the local velocity error is 2nd order accurate.

2.2 Simulation Setup

The slope was created using a script *ContinuousTilt*, which was written by Thomas Weinhardt 7 years prior to this study. The script simulates an open box with particles placed inside. The angle of the box with the ground is then increased every timestep for a long enough time that several avalanches have formed. The script loads a bottom plate from *Bottom.data* for which the particles are fixed in place. It creates an uneven plane on which the particles will be placed. This was chosen in favor of a smooth plate in order to obtain more realistic boundary conditions for the simulation. An avalanche is a flowing layer of debris on top of a slope that is also made of debris; naturally, this slope would not be perfectly smooth.

Once the bottom plate has been made, the flowing particles are generated at random positions above the plate. This study has used 10000 flowing particles, which means that there are 2.5 layers of flowing particles on the plate. This was deemed sufficient through a visual inspection of the created avalanches with Paraview, where it could be seen that only the top 1,5 layers were moving during an avalanche. Furthermore, the impacting particle did not penetrate through the layers far enough to be able to hit the plate. Although more particles could have been added to make the third layer complete, this was not done in view of the simulation duration which increases as $O(n \log(n))$ with the number of particles n . A typical computing time for a single simulation of 500 seconds is approximately 37 hours with 1 core and node on the Serendipity cluster of the University of Twente.

In this study spherical glass particles were used, for which the specific parameters can be found in table 1. This decision was threefold. Firstly, these values were determined 7 years ago by Thomas Weinhardt, and there was currently no experimental setup available

to determine these values ourselves. Hence the the choice to adopt pre-existing values. Secondly, the particles were taken to be spherical due to the simulation time, which greatly increases with non-spherical particles. Thirdly, the density of glass ($2500\text{kg}/\text{m}^3$) and rock ($2600\text{kg}/\text{m}^3$) are very similar, which could lead to similar results [4].

After the particles are dropped on the plate, they are given time to settle into a packing. Once this is done, the direction of gravity is slowly adjusted to simulate a tilting slope. This was done instead of actually tilting the slope, because the two are mathematically identical. The gravity vector for a given angle α is

$$g = 9.81 \cdot \langle \sin(\alpha), 0, -\cos(\alpha) \rangle \quad (5)$$

as can be derived from the image below. The slope angle α is increased by $2 * 10^{-6}$ every simulation timestep of $1 * 10^{-4}\text{s}$. It was chosen to output every 0.5s to limit the size of the output file. The script outputs the positions, velocities, radii, and angular velocities of each particle in a .data file, as well as the kinetic, elastic and rotational energies of the system in a .ene file for every chosen timestep.

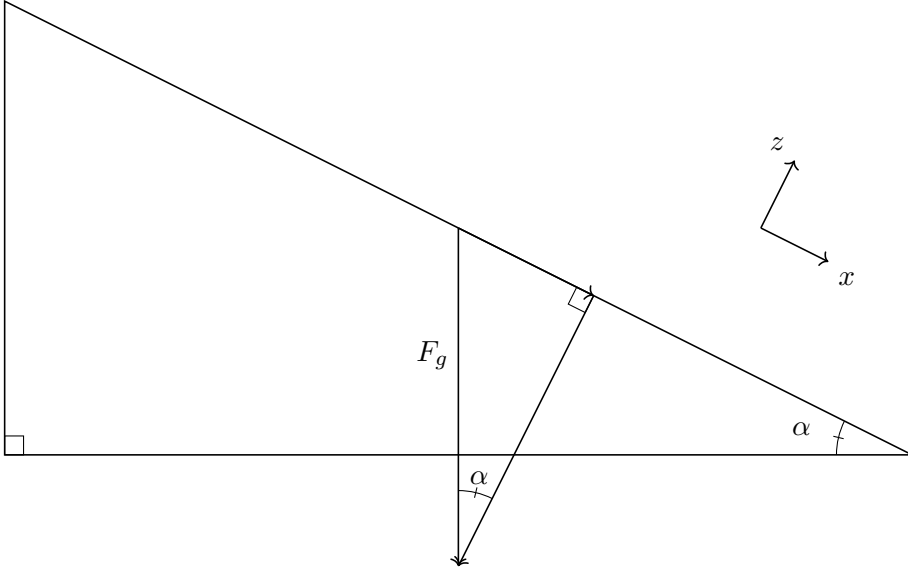


FIGURE 2: A schematic diagram of a slope tilted at angle α . In the simulation the coordinate system is rotated parallel to the slope in the (x,y) plane.

2.2.1 Walls

As shortly mentioned in the previous section, the plate on which the particles are dropped is inside an open box of dimension 0.8m by 0.6m by infinity. This means that there are walls at the sides, top and bottom of the slope. The wall at the top of the slope has no influence on the avalanches and is solely used to prevent the particles from falling off the slope during its generation. The walls at the sides could potentially influence the avalanches, since they restrict the movement of the particles near the sides. However, this can be neglected, because of the nature of this experiment. The experiment concerns whether an avalanche starts, not how it is shaped. Through visualisation using Paraview it was observed that avalanches only approach within 5 particles of the side walls after the maximum kinetic energy has been reached. This leaves the possible influence from the bottom wall. The bottom wall stops the particles from falling off the slope during an avalanche. This causes

the particles first couple of particles that reach the wall to bounce back up, thus influencing the particles coming after them. However, the wall is quite elastic, so there is some delay between hitting the wall and bouncing back during which time the next set of particles has mostly reached the wall. In combination with the fact that this only influences the speed of a few particles after the avalanche has already reached the bottom, the bottom wall does not interfere with the nucleation of avalanche. Therefore, the walls do not have sufficient influence on the creation of an avalanche.

2.3 Avalanche nucleation criterion

There are several ways to determine the presence or absence of an avalanche in Mercury-DPM, such as in terms of the kinetic energy of the system and the center of mass. The kinetic energy is a possibility, since the particles in an avalanche would speed up as they fall down further, as well as causing more particles to start falling down, thus increasing the kinetic energy until the wall at the bottom of the slope is reached. If there is no avalanche, one would expect the kinetic energy of the system to remain at 0. If there is an avalanche, one would expect a peak in the kinetic energy at some point in the time that the avalanche was moving. Similarly, for the center of mass one would expect that it stays the same if no avalanche occurs. If an avalanche does occur, one would expect the center of mass to shift downhill.

We chose to use the kinetic energy of the system as a measure, since it more clearly depicts the different stages of an avalanche caused by dropping a particle (figure 3). Phases IV and V can still be seen by using the center of mass, but phases I and II cannot. Phase V would be different for a simulation setup without a bottom wall. If there was a gradually flattening surface instead of a wall there would be an exponential decay, but due to the influence of the wall which bounces the particles back, the kinetic energy takes longer to dissipate.

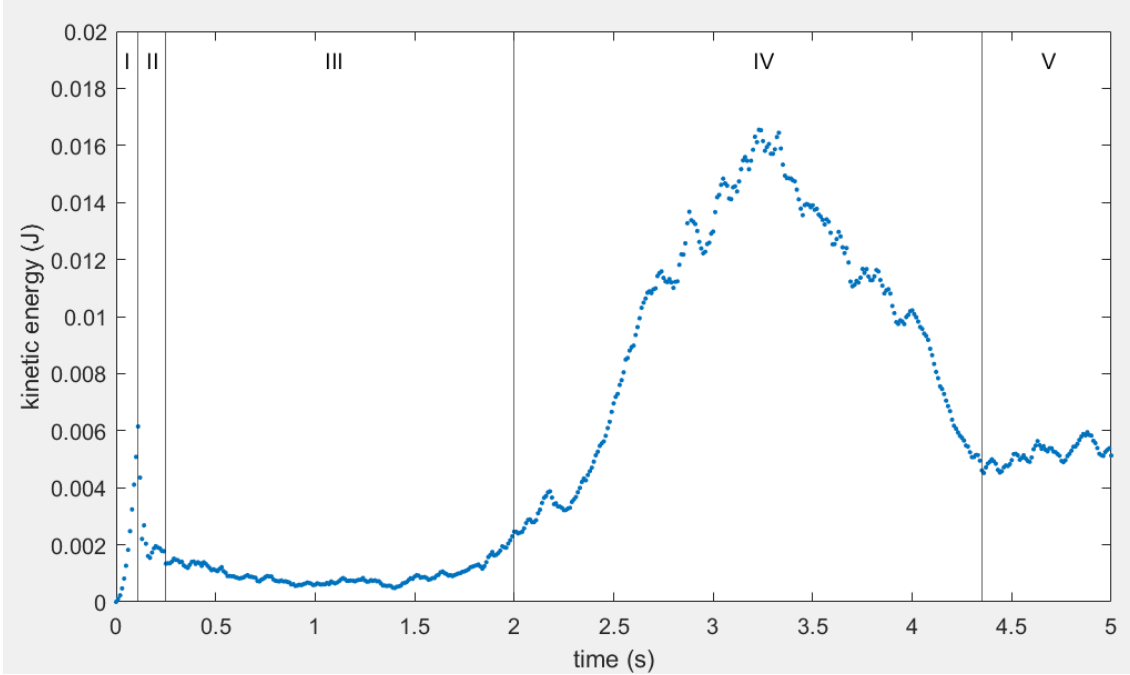


FIGURE 3: The kinetic energy (J) of a system of 10000 particles when a particle is dropped on it and an avalanche occurs over time (s). The cutoffs of the different sections are for illustrative purposes only, the exact location may vary. **I**: The particle is falling, all other particles are at rest. **II**: The particle hits the slope and the kinetic energy is converted into elastic energy during the collision. **III**: The energy is spread out to more particles, but the movements of the particles is small. **IV**: The particles have started to fall down the slope, taking other particles with them causing an avalanche until the wall at the bottom is hit. **V**: The avalanche has stopped, but there are still some particles falling down.

The four images in fig. 4 correspond to the start of I, end of phase III, middle of phase IV and start of phase V respectively. As the more time has passed, the blue and orange areas become larger. The blue area shows the locations where the particles that have fallen down the slope originated from, while the orange area is where they were deposited. Based on several such visualisations of the slope for various measured maximum kinetic energies, the minimum energy required to be termed an avalanche was set to $0.008J$. Movements that occurred with a kinetic energy around $0.005J$ were too small. It either caused an avalanche that stopped halfway down the slope, or only a few particles fell down with a high kinetic energy per particle. These two situations will be referred to as partial avalanches in the rest of this paper.

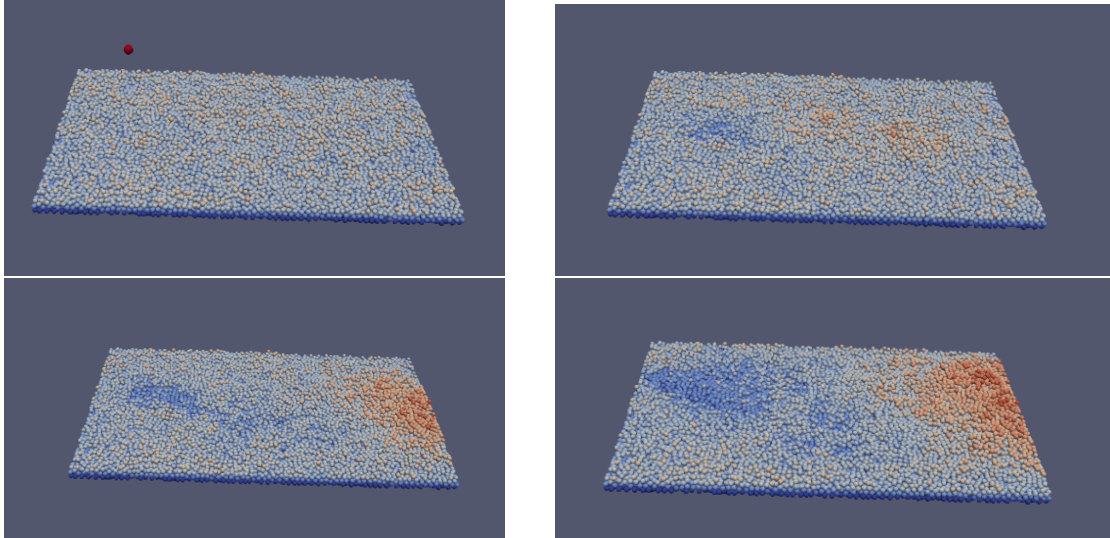


FIGURE 4: The progression of a triggered avalanche in four frames. The colouring is based on the z -position of the particles. **top left:** the impacting particle is released at $t = 0s$. **top right:** the avalanche is beginning to gain momentum at $t = 1.5s$. **bottom left:** the impacting particle as well as the front of the avalanche have reached the bottom of the slope at $t = 3s$. **bottom right:** more particles have continued to fall and have been deposited at the bottom of the slope at $t = 5s$.

2.4 Angle of repose

In order to ensure that the slopes would be in the stable region, it is necessary to first determine the angle of repose. This was done using the *findAngleofRepose* script. This script takes a slope at a given angle as generated by *ContinuousTilt* during some timestep and lets it rest to determine whether or not an avalanche could occur naturally. The time was set to 20 seconds after determining that most natural avalanches occur within 10 seconds, but an occasional avalanche started after 15 seconds. The range of angles to check for the occurrence of a natural avalanches was chosen by plotting the kinetic energy of the system from *ContinuousTilt*, which showed that the first avalanche occurred at approximately 18.25° (fig. 5). The range was chosen was $18.1^\circ - 18.4^\circ$ in steps of 0.01° , which is centered around 18.25° .

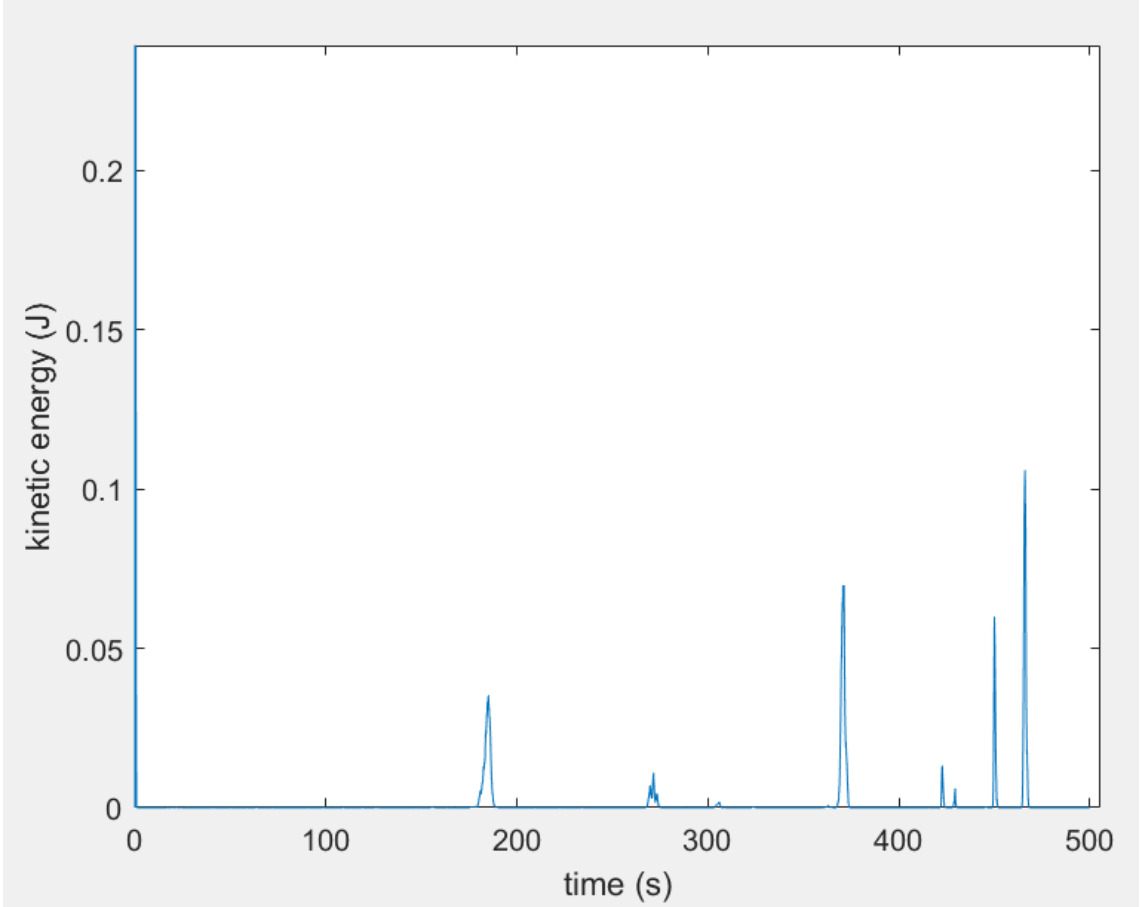


FIGURE 5: The kinetic energy (J) of the system over time (s) as the direction of the gravity vector is slowly changed. The first peak is after approximately 182 seconds, which corresponds to an angle of 18.25° .

2.5 Trigger

The script *Trigger* was used to simulate dropping a particle on the inclined plane. The dropped particle is of the same material as the particles on the slope, but its radius is twice as large (note while the density remains constant, the mass becomes 8 times as large). This was chosen to make the impacting particle hit multiple particles on the slope upon impact, instead of having higher chance of hitting a single particle and transferring its energy only to that particle. The influence of the size of the impacting particle on the occurrence of an avalanche has not been verified. The particle was chosen to be of the same type to ensure that the friction coefficients and other factors dependent on the material could be kept the same as in table 1.

The *Trigger* script takes a .data file, the slope angle and the height from which the particle is dropped as input parameters. The .data file contains the positions, velocities and radius of the particles that make up the bottom plate, flowing particles and impacting particle as produced by *ContinuousTilt*. The slope angle is used to determine the orientation of the gravity vector and must be given in degrees. The drop height is height of the impacting particle perpendicular to the slope (h_\perp in fig. 6); it must be given in meters. It is important to ensure that the drop height of the impacting particle is above the position in the z -direction of the particles on the slope. Since all slopes used in this study consist of 14247 particles, where a single layer consists of at most 4247 particles, and the diameter of each particle is $0.01m$, the drop height was chosen to be at least $0.04m$ to ensure there

is no contact prior to release.

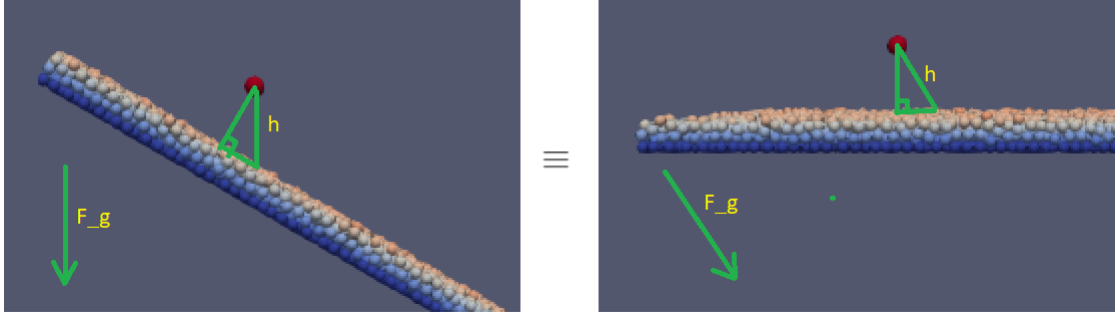


FIGURE 6: Schematic diagram of the distance h that the impacting particle covers when dropped. The left image shows how this works for a tilted slope, whereas the right side shows the equivalent image for a rotated gravity vector.

However, the drop height is not the displacement of the impacting particle during its drop; that is given by h in fig. 6. It is clear that the angle between h_{\perp} and h is the same as the slope angle α . Hence the relation between the two is given by

$$\frac{h_{\perp}}{h} = \cos(\alpha) \quad \text{or} \quad h = \frac{h_{\perp}}{\cos(\alpha)}.$$

This means that, neglecting air resistance, the kinetic energy upon impact scales inversely with $\cos(\alpha)$. In this paper a small range of angles was chosen, since many simulations were needed per angle to find the expected transition. This resulted in a range of less than 1° , which would result in an insignificant difference in the kinetic energy compared to the uncertainty in the exact perpendicular displacement of the dropped particle. This uncertainty is created by the incomplete top layer, causing the possibility for the impacting particle to hit either the top layer or the layer beneath it. The kinetic energy of the impacting particle upon impact can be experimentally determined by running the simulations with a smaller chosen timestep for the output files and determining the energy at the transition between phase I and II.

2.5.1 Range of drop heights

The range of drop heights used was based on what external objects could realistically drop on a mountain slope and potentially cause an avalanche. As such, if the slope consists of baseball-sized rocks the minimum impacting particle considered is a rock the size of a baseball falling approximately 1 meter before impact. The maximum impacting particle considered is a small tree falling 10 meters before impact. This will keep the range of impacting particles within realistic boundaries, as small trees can grow on a flatter part of a mountain slope and then fall down a cliff, while if anything smaller than the falling rock can set off an avalanche the debris would have already started flowing due to a random ground hog.

Neglecting air resistance, the final kinetic energy is equal to the difference in potential energy. Hence the two factors influencing the kinetic energy upon impact are the height from which object is dropped and its mass. This gives kinetic energies of $4.91J$ and $1.16 \cdot 10^3 J$ for the ball and tree respectively. Unfortunately, the author did not have a good enough grasp of MercuryDPM to understand the implications of varying the parameters previously set by Thomas Weinhardt, thus creating the need to scale the kinetic energies to a slope of glass particles with a radius of $0.005m$. This requires scaling in lengths. Kinetic

energy scales directly with h and with volume (thus cubic in the radius), and the radius of a baseball is $0.0365m$. This causes a scaling factor of $(\frac{0.0365}{0.005})^4 = 2.84 * 10^3$, which gives a scaled energy range of $0.0017J - 0.407J$. Since these are estimates, the reasonable range was considered as kinetic energies with the order magnitude of $10^{-3} - 10^{-1}J$.

The slope is not guaranteed to be topographically flat, leading to an uncertainty in the precise kinetic energy upon impact. Hence, a range of drop heights was favored over kinetic energies; the kinetic energy was subsequently determined from the simulations as described in section 2.5. The drop height range that was used is $0.04m - 0.4m$. This corresponds to an approximate range of $0.001J - 0.038J$ for the kinetic energy upon impact, which is at the very bottom of the plausible range. This underpins the fact that this study is focused on slopes tilted at angles very close to the angle of repose. After an initial test of *Trigger*, it was determined that avalanches started as low as a drop height of $0.06m$ for 18.1° on slope A, and no significant change in the maximum kinetic energy was detected in the avalanches for lower or higher heights. Therefore, a larger range of heights would only be needed once a broader range of angles further away from the angle of repose was selected. Due to time constraints, it was necessary to strictly limit the number of simulations.

2.6 Horizontal shift

To verify whether the topographical influence was negligible, the script *TriggerShift* was used. It is based on the *Trigger* script, with the addition that the y -position of the impacting particle can be adjusted. It was used to determine the presence or absence of both local and regional topographical influence on the occurrence of avalanches.

Local influence refers to how the impacting particle hits the particles on the slope. It was inspected because a number of the results deviated from what was expected. One of these deviations is that occasionally no avalanche occurred for a certain drop height after avalanches were already observed for several lower drop heights at that slope angle. It is important to determine what the cause is to develop a method to mitigate the prominence of these outliers. Since these outliers differ from the behaviour around them, it is unlikely to be due to the slope itself. Another option that could cause this is if the landing of the particle has influence on the occurrence of an avalanche. Does it matter if it hits a particle on its left side or right side versus in the middle? As such, the range was chosen to have a breadth of 2 diameters (of the particles on the slope), or $0.02m$, with a stepsize of 0.001 , which is equal to 0.1 radius.

Regional influence refers to where the impacting particle lands. It was investigated because of the randomization in the packing of the slope. Since the packing is random, the topography of the top layer can be skewed with more particles in some places and less in others. This could then cause some (x, y) -positions for the impacting particle to result in the particle falling in a small hill or valley. To verify the possible influence of the drop position on the nucleation of an avalanche, the particle was dropped at various y -positions for a fixed drop height and slope angle. The range of angles was set to $0.24m - 0.36m$, which is six diameters to the left and right of the center position. No variation was done for the x -position as this also influences the length of the slope that can be traversed before the bottom wall is reached. This could negatively affect the maximum kinetic energy in an avalanche causing it to be below $0.008J$.

3 Results

This section contains the results and further refinements made in view of those results. In section 3.1 it was assumed that the topography of the slope had no influence on the occurrence of an avalanche. This was determined to be incorrect, leading to additional research into the amount of influence the topography has. As such, the results from section 3.1 can be considered relevant for only that slope, while the more general conclusions can be made from section 3.2, where the topographical influence is discussed in more detail.

3.1 Slope A

Slope A was created by running *ContinuousTilt* with *random.randomise()* turned off in the code.

3.1.1 Natural avalanche

In order to ensure that the slope was in the stable range, the angle of repose was determined as described in section 2.4 with the angles ranging from 18.1° to 18.4° . The results obtained are displayed in fig. 7.

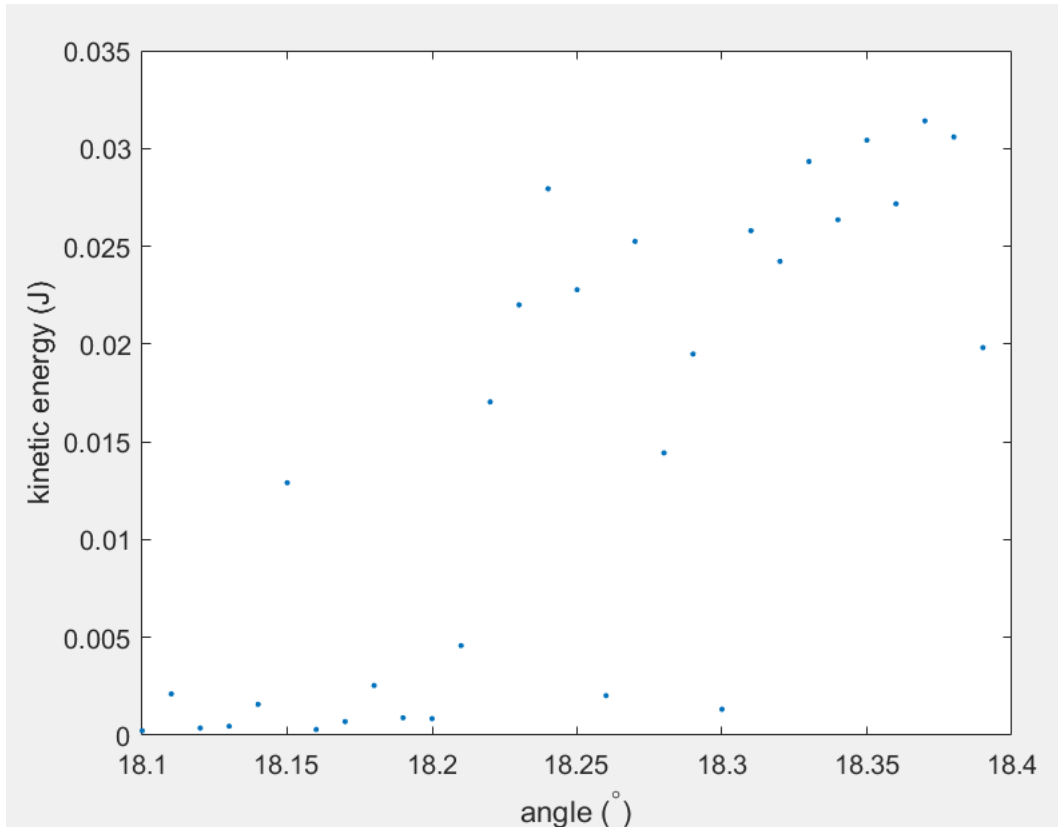


FIGURE 7: The maximum kinetic energy (J) that occurred per angle ($^\circ$) when the gravity vector was rotated until that angle was reached; the slope was then fixed at that angle and left alone for 20s.

There is a clear qualitative change present in fig. 7, around 18.22° , which corresponds to what was expected based on fig. 5. There are three points that deviate from the norm, namely for 18.15° , 18.26° and 18.30° . These simply indicate that the region very close to the angle of repose is not clear-cut stable or unstable, but sensitively depends on the

packing of the grains. Since the slopes in the region of $18.1 - 18.2^\circ$ are all stable with the exception of 18.15° , where the avalanche only occurred after 15 seconds, the range for the triggered avalanches was set to a maximum of 18.1° .

3.1.2 Triggered avalanche

For each angle the *Trigger* script was run to determine the necessary kinetic energy to cause an avalanche. There is a marked transition in the maximum kinetic energy of the system, in this case as a function of the drop height of the impacting particle (fig. 8 (left)). Similar to fig. 7, the region very close to the critical drop height can contain points where an avalanche occurs while below the critical height or not occur above it. It can be seen in fig. 8 (right) that the unexpected avalanche at $h = 0.14m$ has a longer delay and a smaller magnitude than the other avalanches. This is characteristic for the avalanches that occur below the critical height, as the particles in the avalanche have less energy left over to cause other particles to start falling as well. It also takes longer for the particles to gather speed, as they have just enough energy to overcome friction and the small height barrier created by the particles in front of them, thus creating a delayed, smaller avalanche.

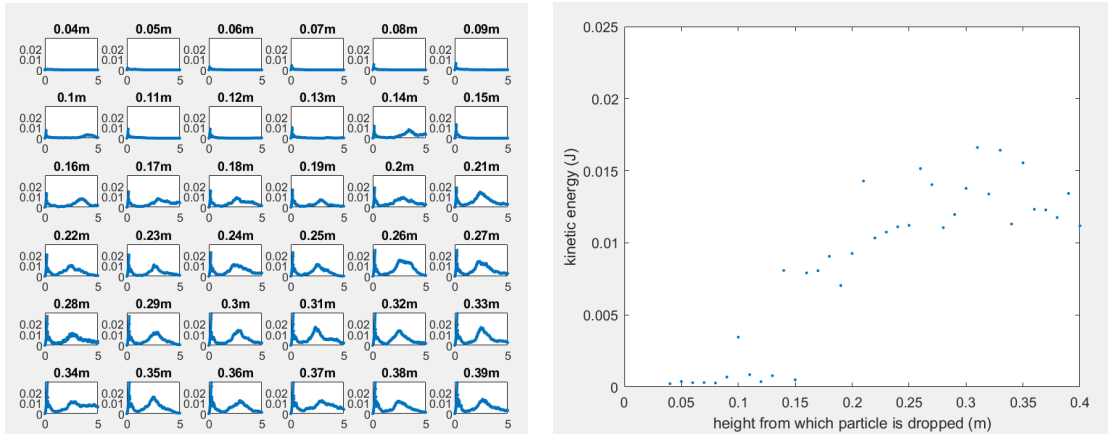


FIGURE 8: Each subplot shows the kinetic energy (J) of the system over time (s) for $\alpha = 17.8^\circ$ (left) over a range of drop heights. The maximum kinetic energy for each drop height for $\alpha = 17.8^\circ$ (right).

It can also be seen that the maximum kinetic energy continues to increase as the drop height increases after the the critical height is passed. This relation appears to be linear, but in the region from 0.25 to 0.35m the maximum kinetic energy fluctuates considerably, indicating that there should be other factors influencing the relation between the maximum kinetic energy and the drop height.

In the search for what could be causing the deviations from the critical drop height, and out of necessity of verifying the assumption that the precise topography of the slope is irrelevant to the nucleation of an avalanche, *Trigger* was applied for 13 different y -positions for the impacting particle as seen in fig. 9.

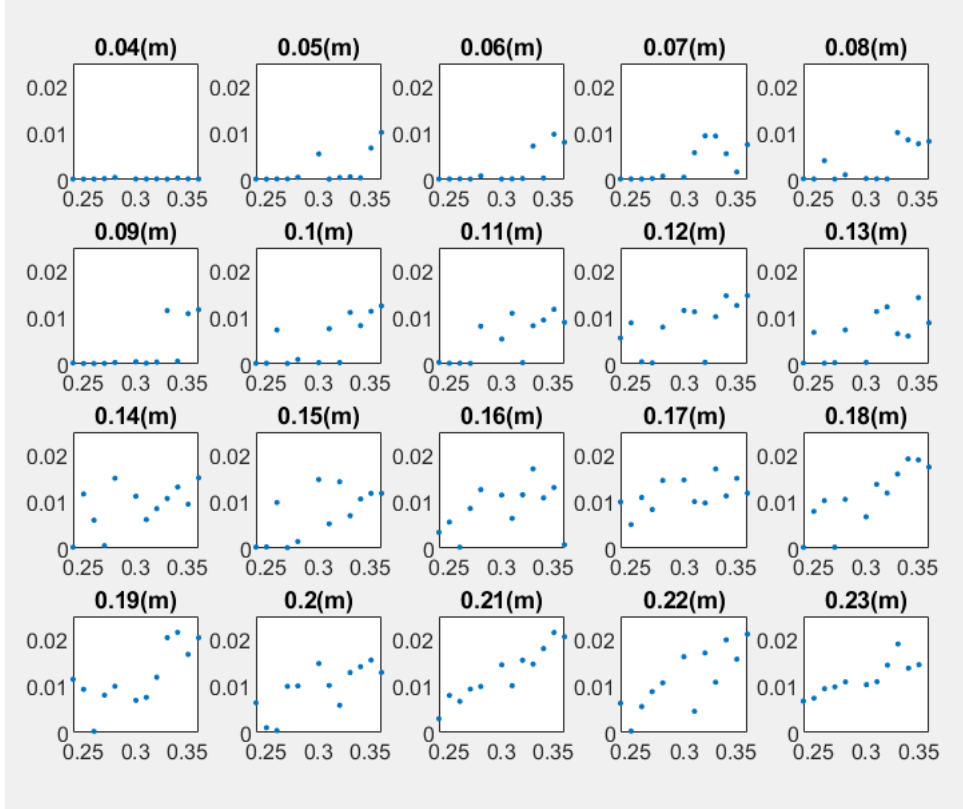


FIGURE 9: Each subplot shows the maximum kinetic energy (J) as a function of the y -position of the impacting particle (m) for a given drop height (m). The drop height is shown as label for each of the sub-plots, whereas the y -position was varied between 0.25 and 0.35 m.

A quite concerning pattern can be seen in these subplots. If the topography of a slope was irrelevant to the nucleation of avalanches, it would be expected that either an avalanche would occur for all y -positions for each given drop height or for none. Instead, it can be seen that the lower y -positions, which are on the left side of the slope, and the higher y -positions, which are on the right side of the slope, do not show the same behaviour at all. Additionally, even when an avalanche does occur for all y -positions, such as for a drop height of 0.23m, the maximum kinetic energy is still higher for the right side than the left side. This could have two reasons. Firstly, the slope is different on the left side than on the right side, and the topography does influence the occurrence of an avalanche. Secondly, there is an error in the code which causes a dependence on the y -position for the occurrence of an avalanche. This second assumption was checked by mirroring the slope on $y = 0.3m$, and shown to be incorrect (see appendix C). As such the topography clearly does influence the avalanche nucleation, making the assumption invalid.

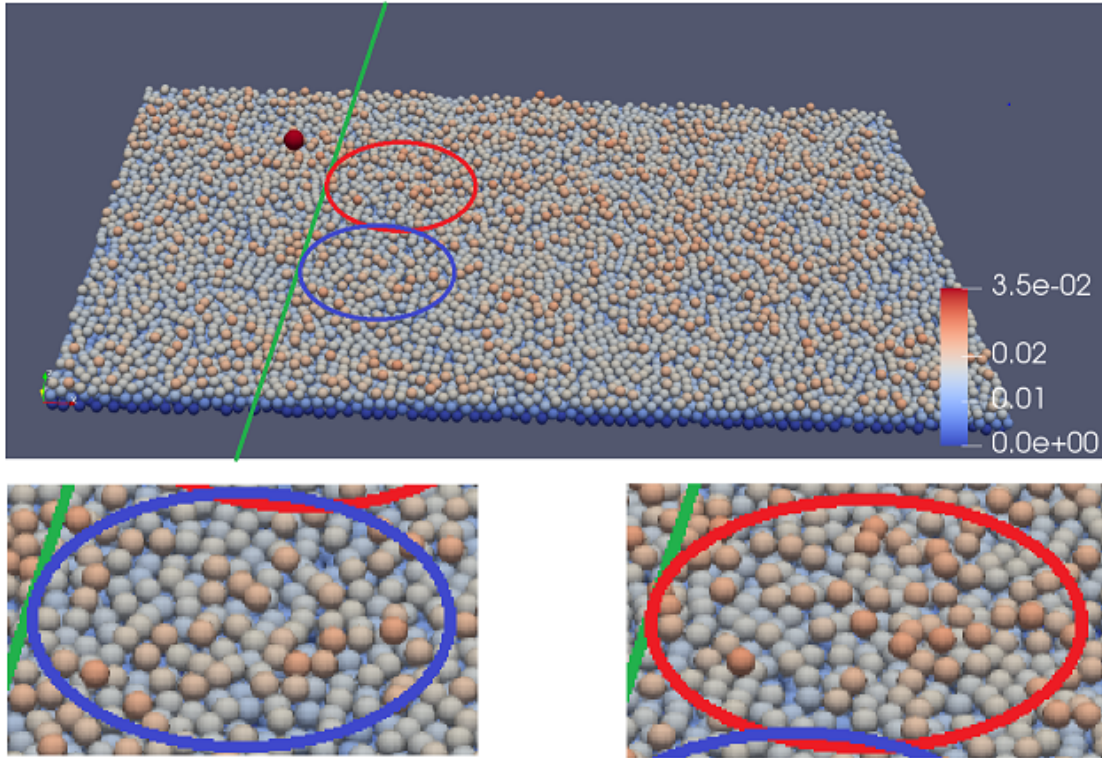


FIGURE 10: The slope at 17.91° in Paraview. The green line displays the x -position the impacting particle will hit the slope at for varying y -positions when dropped from $0.09m$. The red circle is the right side of the slope and the blue circle is the left side of the slope. The particles are coloured based on their z -position.

A topographical difference between the left and right side was verified by looking at the starting frame in Paraview (fig. 10). This showed that the particle was hitting the slope in a small dip on the left side; upon impact the particle pushed the few orange-colored particles in front of it, thus quickly creating a barrier it could not overcome. On the right side this also occurred, but due to the presence of more orange-coloured particle the particles started to gather speed instead of staying still, thus facilitating the creation of avalanches. From this, it could be expected that all drops on the left or right respectively should show the same behaviour. Taking a closer look at this shows that while there is a clear difference between the left and right side, there are also y -positions where the result does not conform to the surrounding results.

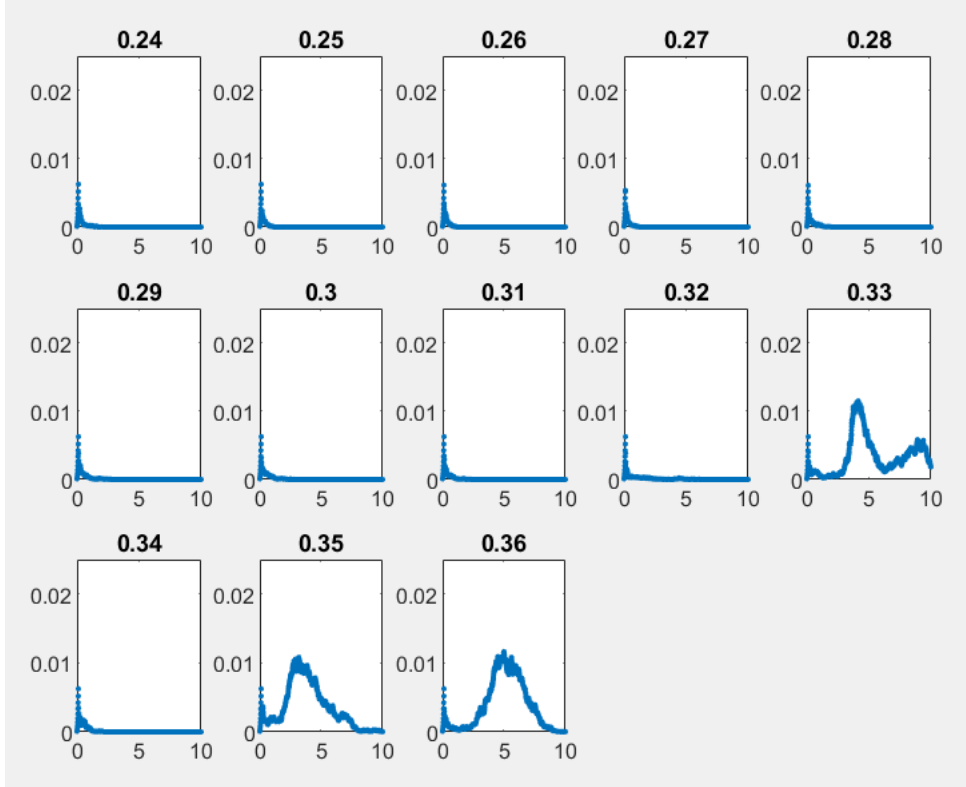


FIGURE 11: Each subplot shows the kinetic energy (J) of the system over time (s) for a given y-position in meters where the particle was dropped from 0.09m for $\alpha = 17.91^\circ$.

In fig. 11 it can be seen that there are no avalanches on the left slope or middle and some avalanches on the right slope. However, there is no avalanche for 0.34m. This would indicate that there is not only a regional topographical influence, but also a possible local influence. If this local influence does indeed exist, then by shifting the y-position a fraction of a radius from 0.34m should cause an avalanche, thus showing the regional influence.

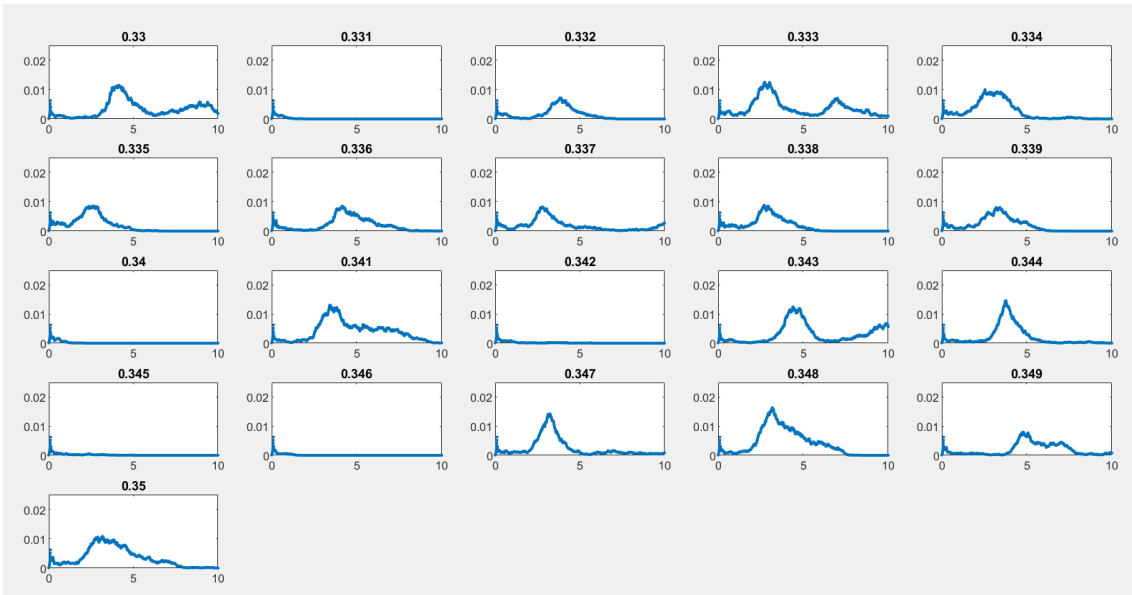


FIGURE 12: Each subplot shows the kinetic energy (J) of the system over time (s) for a given y-position in meters where the particle was dropped for $\alpha = 17.91^\circ$.

This was tested as shown in fig. 20, where a range from 0.33 to 0.35m was taken in steps of 0.001m, which is $1/5th$ of a radius. It can be seen that there are indeed avalanches occurring around 0.34m, thus suggesting that there is considerable sensitivity to the development of an avalanche on the actual local configuration in case of slopes close to the angle of repose. There are a total of 5 out of 21 y-positions where an avalanche did not occur. They are fairly randomly distributed throughout the 21 locations, suggesting that the local influence on a simulation result could be mitigated by taking a small number of locations very close to the original location and taking the majority to be what would occur if the local influence did not exist. However, this has yet to give a clear result for the amount of influence the regional differences could cause. Several different slopes were made for this purpose, for which the results will be discussed in the next section.

3.2 Topographical influence

Four additional slopes were made with a different random placement of the 10000 particles at the beginning of *ContinuousTilt*. The simulation results from three of these slopes for the natural avalanches and the triggered avalanches were compared. The fourth slope was excluded after trying to find the angle of repose, which appeared to be at a higher angle than the other slopes as well as the fact that avalanches occurred at angles far below the apparent angle of repose. This can be found in appendix B.

3.2.1 Natural avalanches

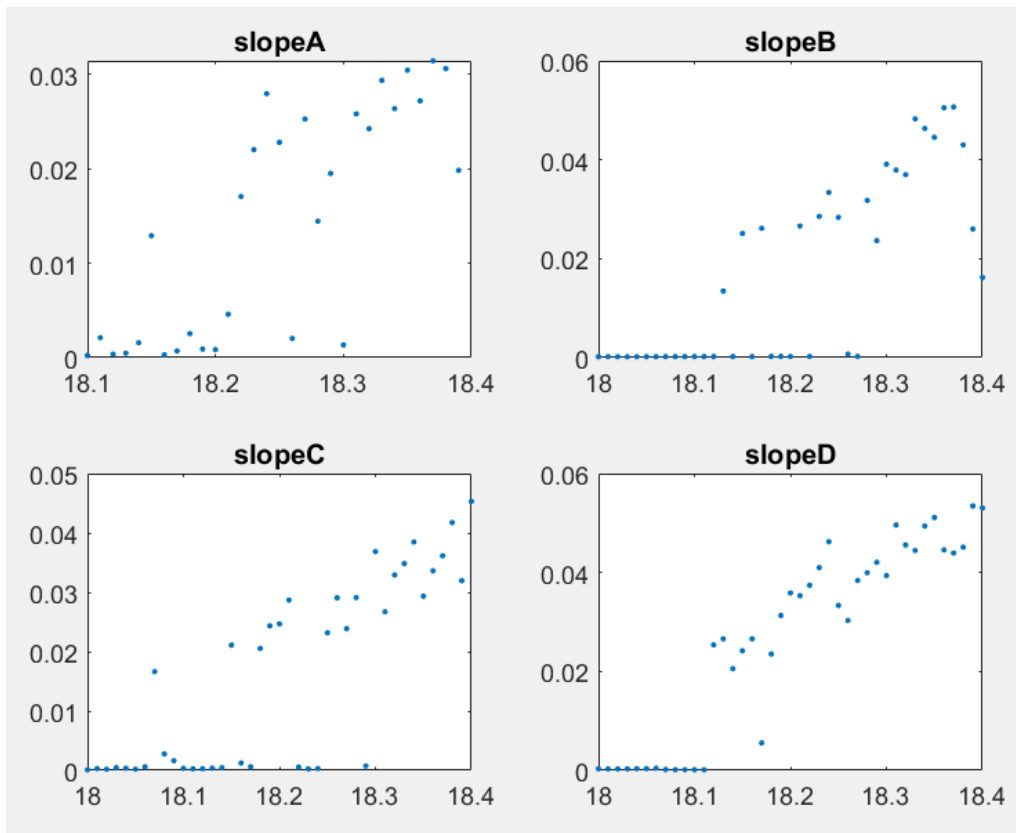


FIGURE 13: The maximum kinetic energy (J) that occurred when the slope was fixed at a given angle ($^{\circ}$) and left alone. Slope A is the original slope, slopes B, C and D were newly rendered.

There are two notable phenomena in fig. 13 that could not be seen previously. Firstly, the transition does not occur at the same angle for all 4 slopes. For slope A it is at 18.22° , for slope B it is between 18.15° and 18.21° , for slope C it is at 18.18° , and for slope D it is at 18.12° . The transition occurs at smaller angles for the three new slopes, but all the values fall within a range of 0.1° of each other. Also, the exact location of the transition is less clear for slope B, since there are some angles where an avalanche occurs while the angles directly above them do not have an avalanche. Therefore, it can be concluded that the angle of repose is dependent on the packing of the slope.

Secondly, beyond the angle of repose the maximum kinetic energy increases as the angle increases. There are clearly fluctuations, but the general trend shows a linear correlation between the angle and the maximum kinetic energy. Beyond the small range of angles included here, it is plausible that the increase would slow down and eventually stop when extending the range range of angles, since there is only a limited number of particles on the slope. Hence, there is a limit on how high the maximum kinetic energy can grow; the increase in the energy will decrease as the values approach this limit. This would be difficult to verify with the current setup, because an avalanche will occur while the slope is still being tilted, which is how the approximate location of the angle of repose was determined. This problem could be circumvented by directly constructing a slope tilted at those angles. This does have the drawback that it is necessary to construct a tight packing in the down hill direction in the bottom layers, since that is what would have otherwise occurred during the tilting process.

3.2.2 Triggered avalanches

To ensure that the avalanches are triggered in the same location for each drop height and angle, the x -position of the impacting particle needs to be adjusted depending on the drop height and angle. As the impacting particle falls it covers a distance parallel to the slope (h_{\parallel}) in fig. 6. It can clearly be seen that the relation between the drop height h_{\perp} and h_{\parallel} is given by

$$\frac{h_{\parallel}}{h_{\perp}} = \tan(\alpha) \quad \text{or} \quad h_{\parallel} = h_{\perp} \tan(\alpha).$$

Therefore, to cause all particles fall on the same region to ensure that the same regional influence is present for all drop heights and angles, the x -position of the impacting particle is set to shift $h_{\perp} \tan(\alpha)$ uphill from its position $3/4^{th}$ up the slope. This was not done for slope A, making it impossible to compare that slope with the other three for the triggered avalanches.

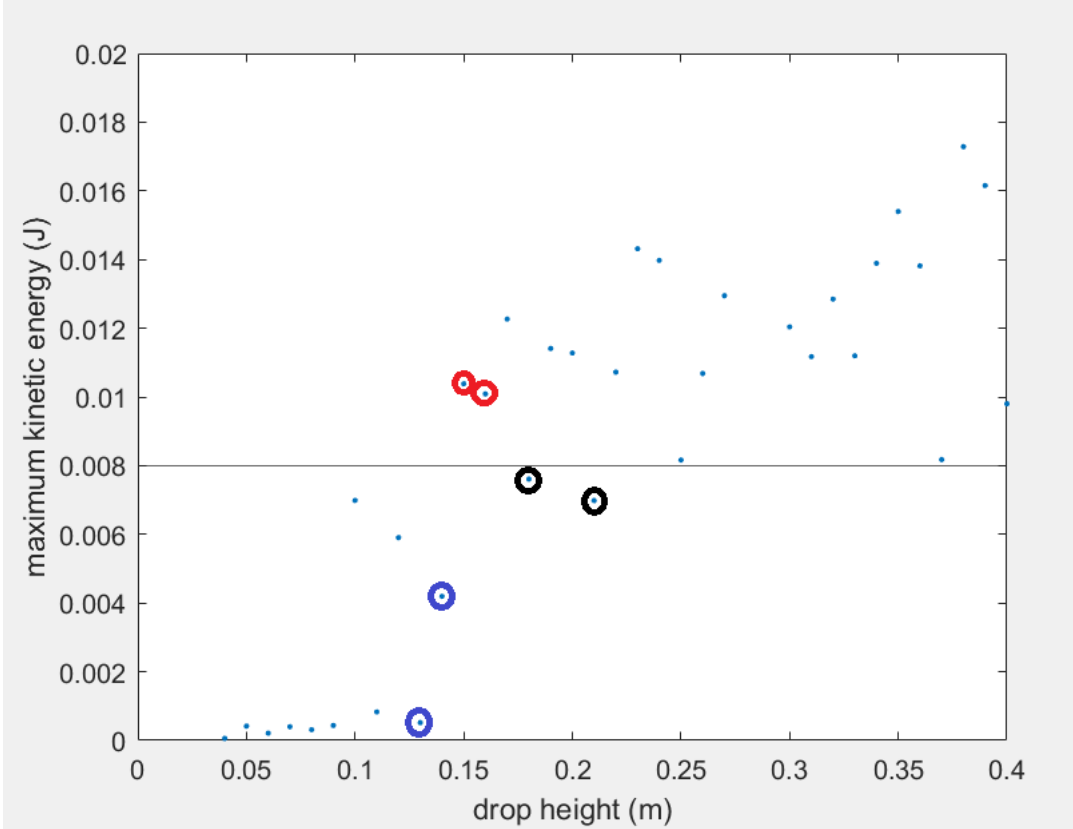


FIGURE 14: The maximum kinetic energy (J) is plotted against the drop height (m) for a slope angle of 17.6° on slope C. The horizontal line at $0.008J$ is the cutoff line for an avalanche. The blue and red circles represent the transition from the absence to the presence of an avalanche. The black circles show two deviations from that transition.

In order to compare the critical drop height across angles it was necessary to choose a method for determining the location of this critical height. Simply using the kinetic energy criterium of $0.008J$ did not provide a clear choice of critical height. This can be seen in fig. 14 where the black circles indicate drop heights for which no avalanche occurred even though a visual inspection would have placed the critical height below these drop heights. These deviating results could be caused by the local influence found in section 2.5. To reduce the influence of these outliers the transition location was determined using a requirement of two consecutive kinetic energies below or above $0.008J$. The two blue circles indicate the last two consecutive energies below $0.008J$, thus making the higher of the two drop heights the bottom of the critical height range. The two red circles indicate the first two consecutive energies above $0.008J$, making the lower of the two drop heights the top of the range. Ideally, the blue drop height should always be below the red drop height. Unfortunately, there are times when this does not happen. This is could have happened in fig. 14 if the two black circles had been consecutive as well, and it can be seen that this did happen in fig. 15. Using the method described in section 2.5 to mitigate the influence of the local topography could reduce the distance between the red and blue drop heights and potentially flip them to the right order. One instance where that might be useful is for slope angle 17.76° for slope B.

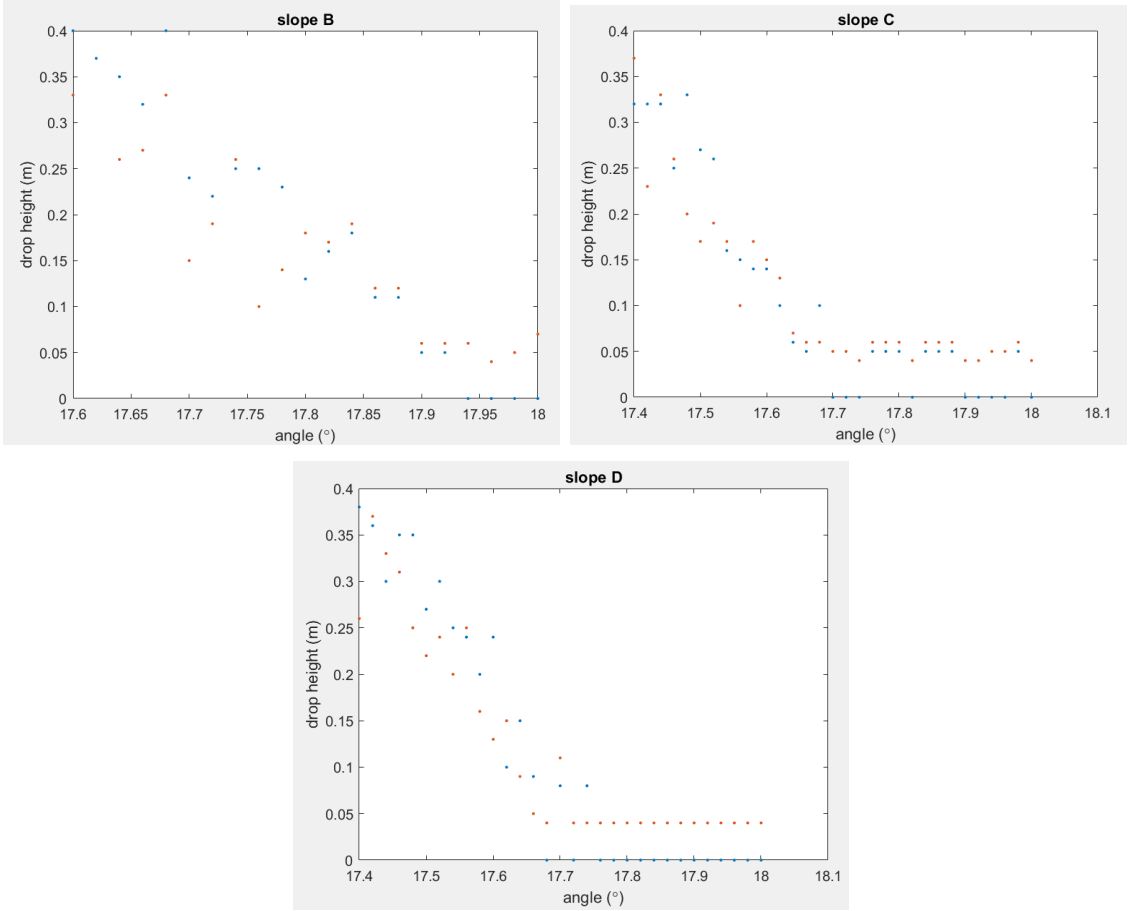


FIGURE 15: The critical drop height (m) is plotted against the slope angle ($^{\circ}$) for slopes B, C and D. The blue dots are the last consecutive energies below $0.008J$, and the red dots are the first consecutive energies above $0.008J$. If avalanches occurred for all drop heights, the blue dot was placed at $0m$.

A clear relation between the angle and critical drop height can still be seen for all three slopes in fig. 15. All three subplots show that once the slope angle is sufficiently small that avalanches do not occur at the bottom of the drop height range ($0.04m - 0.06m$) the critical drop height increases linearly as the the slope angle decreases. The rate at which this happens is similar for all three slopes; the critical drop height increases with approximately $0.4 - 0.05 = 0.035m$ for a decrease of 0.3° . This is quite remarkable, because the maximum kinetic energy vs drop height plots for the three slopes looked a bit different, making it unexpected that the rates would be so similar. Besides the similarities there is also one main difference between the three subplots. For slope B the linearity is observed from 17.6° to 17.9° , while it is observed from 17.4° to 17.7° for slopes C and D. Some difference is not very surprising as the angle of repose is also earlier for slopes C and D than for slope B. However, the difference in the angle of repose is smaller than the difference observed here, indicating an additional cause for the difference. One possibility is that the impacting particle hits a hill for slope C and D and/or a valley for slope B. This could be verified as done described in section 2.6.

4 Discussion

In this paper the influence of dropping a particle on a stable slope of glass beads was investigated. This led to the discovery of several phenomena of which the most important is that the results depend strongly on the topography. Firstly, the value of the angle of repose found in this study is between 18.12° and 18.22° , which deviates from what was expected where the angle of repose was located at 25° for 2-3 layers of free particles [5]. There are some differences and similarities between the experiment done in this paper and that of Forterre and Pouliquen. The differences are that they did the experiments in reality instead of with simulations, used smaller particles and started with a uniform layer of particles. The similarities are that both used glass beads, a tilting inclined plane to find the angle of repose and a rough bottom constructed by gluing beads to a bottom plate. Of these differences, it is presumed unlikely for the size of the beads to influence the angle of repose this much, since this would imply that the experiments done on chutes, piles and inclined planes would not scale to larger particles of the same material in reality. Of course, it is possible for a scaling factor to exist which would make the scaling possible, but it would be unlikely for it to cause a deviation of more than 20% in the value for the angle of repose. This leaves the possibility of large differences between reality and the simulation method, but there exist a significant number of papers where a similar model is used for simulations which is then verified with experiments. As such, the proposed cause of the large difference is the incompleteness of the top layer in this paper; the paper of Forterre explicitly states that they start with a uniform layer of particles. A possible explanation would be that the incompleteness of the top layer makes it possible for a higher slope angle to exist locally. This angle could then correspond to that of Forterre and Pouliquen. This can be verified by repeating the simulations with more particles to create a full 3 layers. Naturally, other factors such as different friction coefficients, dissipation and air resistance can also be the cause. This can be tested by using the values from Forterre and Pouliquen in the simulation model.

Secondly, the transitions for the natural avalanches are much clearer than those for the triggered avalanches. For the natural avalanches the behaviour was as expected; there was either no motion or a full layer would flow down the slope. The same was expected for the triggered avalanches, and this definitely did occur for part of the simulations. What differed from the expectations is that partial avalanches also happened on occasion. This makes it difficult to determine where the border for avalanche/no avalanche is located, which in turn makes a clear relation between the angle and the amount of energy necessary to cause an avalanche to be unclear. This is further exacerbated by the influence of the location at which the impacting particle hits the slope. This influence can be decreased by shifting the drop location by a fraction of the radius as done in section 3.1.2 and taking the more prevalent result as 'correct'.

Thirdly, the regional topographical influence on the occurrence on avalanches is strong. This is possibly caused by the incomplete top layer which facilitates the creation of small dips and hills by the presence or absence of the particles in the top layer in a small region. In this case, this can be verified by creating several slopes with a tightly packed third layer, similar to for the angle of repose, and to then repeat the simulations in this paper. Although this also introduces a change in the number of movable particles, it should still be usable for this verification.

Fourthly, although the topological influence interferes with a quantitative comparison between different slopes, a qualitative evaluation is still possible. This was seen in section 3.2.2 in the type of behaviour shown by slopes B, C and D, which was the same. The

slope angles that behaviour occurred at was not the same, and further research is necessary to determine the exact causes of the difference. Several suggestions were done, including a partial cause due to different angle of repose. Additionally, different regional influences on the different slopes was considered. This could be verified by either making several slopes with a tight packing on the third layer, or by taking a more visual approach and finding a similar region on each of the slopes and dropping the particle there to see if the differences in fig. 15 decrease. This has several drawbacks, among which the need for the region to be fairly centralized in the y -position to avoid an increase in the influence of the side walls, as well as an x -position sufficiently high up the slope so that the particles have enough time to gather speed before reaching the bottom wall.

Lastly, due to the small range of angles simulated in this paper, the linear relation found in section 3.2.2 might not be exactly linear. As mentioned, the kinetic energy upon impact is actually dependent on the slope angle, but due to the small range and other factors this was deemed irrelevant for this paper. However, this means that the relation in fig. 15 could also be linear in $\cos(\alpha)$, $\sin(\alpha)$ or $\tan(\alpha)$ as they can be reasonably approximated as linear for the used range of angles. Unfortunately, no methods for verifying which is correct are currently known to the author, as increasing the angle range until the linear approximation is no longer acceptable may not be a viable option. This is because the behaviour of the particles could change angles below θ_{stop} . Another option would be to make the results more precise, but due to some unavoidable randomness, this would require simulations for many different slopes until a statistical approach could be taken. Considering the time required for a single triggered simulation is 50 minutes, this would quickly take a very long time.

5 Conclusion

In this paper we investigated various phenomena that occurred when a particle was dropped on an inclined plane below the angle of repose. This was done through simulations in MercuryDPM. Although no quantitative relation was found between the slope angle and the necessary kinetic energy to start an avalanche, there were some discoveries regarding the trend of this relation. The maximum kinetic energy in an avalanche increases as the slope angle increases. It does not scale with the drop height, rather it stays constant as the drop height increases at drop heights greater than the critical drop height. More importantly, while the topography of the top layer has a strong influence on the occurrence of an avalanche at a given angle and drop height, it does not change the behaviour of the avalanches. It can influence the magnitude of the avalanches, but the shape of the kinetic energy in the system over time remains the same. The qualitative relation between the slope angle and the critical drop height was also the same for slopes B, C and D, indicating that while the influence of the topography is strong for individual simulations, it is not for qualitative behaviour. It can also be concluded that slopes situated at angles very close to the angle of repose are highly unstable. Depending on the slope, a single glass bead dropped from a diameter length above the slope was sufficient to start an avalanche. Additional research needs to be done to determine the causes for the deviations in this study as well as to determine the influence of other parameters such as the radius of the particles, number of layers and particle material. This study can also be further extended to determine whether the behaviour of the triggered avalanches changes once θ_{stop} is reached, as the range of angles used in this study lies between θ_{start} and θ_{stop} . This would enable a better prediction of the instability of a slope, thus possibly aiding in timely evacuation of areas that will face an avalanche in future. Should this be done, it would be nice to use a Savage-Hutter type model to predict the flow of the avalanche to limit which areas need to be evacuated, as well as creating a theoretical bridge between this paper and other research.

References

- [1] Cedar Strip Boat Construction. Wood density chart. <https://cedarstripkayak.wordpress.com/lumber-selection/162-2/>.
- [2] A. Daerr and S. Douady. Two types of avalanche behaviour in granular media. Nature, 399:241–243, 1999.
- [3] Y. Forterre and O. Pouliquen. Flows of dense granular media. Annual Review of Fluid Mechanics, 40:1–24, 2008.
- [4] University of British Columbia. Geophysics foundations: Physical properties: Density. <https://www.eoas.ubc.ca/ubcgif/iag/foundations/properties/density.htm>.
- [5] O. Pouliquen and Y. Forterre. Friction law for dense granular flows: Application to the motion of a mass down a rough inclined plane. Journal of Fluid Mechanics, 453:133–151, 2002.
- [6] S.B. Savage and K. Hutter. The dynamics of avalanches of granular materials from initiation to runout. part i: Analysis. Acta Mechanica, 86:201–223, 1991.
- [7] Julius Vandersteen. How to calculate the volume of a baseball, April 2017. <https://sciencing.com/calculate-volume-baseball-8295708.html>.
- [8] Thomas Weinhart, Luca Orefice, Mitchel Post, Marnix P. van Schrojenstein Lantman, Irana F.C. Denissen, Deepak R. Tunuguntla, J.M.F. Tsang, Hongyang Cheng, Mohamad Yousef Shaheen, Hao Shi, Paolo Rapino, Elena Granonio, Nunzio Losacco, Joao Barbosa, Lu Jing, Juan E. Alvarez Naranjo, Sudeshna Roy, Wouter K. den Otter, and Anthony R. Thornton. Fast, flexible particle simulations — an introduction to mercurydpm. Computer Physics Communications, 249:107129, 2020.
- [9] Wiki. Leapfrog integration, April 2020. https://en.wikipedia.org/wiki/Leapfrog_integration.
- [10] Wiki. Verlet integration, December 2020. https://en.wikipedia.org/wiki/Verlet_integration#Velocity_Verlet.

A Methods

All forces and torques hold for particle i . All variables (unless otherwise specified) are for the current timestep. As stated before, the only external force is gravity which is given by

$$F_i^g = m_i g \quad (6)$$

where m is the mass of the particle and g is the acceleration due to gravity. The internal forces due to contact are elasticity and sliding friction. Both the elastic and frictional forces are dependent on the stiffness and dissipation. These are given by

$$\gamma = -\frac{m}{t_c} \ln(\epsilon) \quad (7)$$

$$k = \frac{m}{2} \left(\frac{\pi^2}{t_c^2} + \frac{\gamma^2}{m^2} \right) \quad (8)$$

where γ is the dissipation and k is the stiffness. Both forces are modelled as spring-damper systems. The variables depend on the relative position r_{ij} , its unit vector n_{ij} , and the elastic deformation δ_{ij} . These are given by

$$\begin{aligned} \vec{r}_{ij} &= \vec{r}_i - \vec{r}_j \\ \vec{n}_{ij} &= \frac{\vec{r}_{ij}}{|\vec{r}_{ij}|} \\ \delta_{ij} &= (a_i + a_j) - |\vec{r}_{ij}| \end{aligned}$$

where a_i and a_j are the radii of particles i and j respectively, resulting in an elastic force of

$$\vec{F}_{ij}^E = [k\delta_{ij} - \gamma(\vec{v}_i - \vec{v}_j) \cdot \vec{n}_{ij}] \vec{n}_{ij} \quad (9)$$

where \vec{v}_i and \vec{v}_j are the velocities of the centers of mass of the corresponding particles. The force due to the sliding friction depends on the sliding stiffness and dissipation, which were determined according to

$$\begin{aligned} k_{sl} &= \frac{2}{7} k \frac{\pi^2 + \ln(\beta)^2}{\pi^2 + \ln(\epsilon ps)^2} \\ \gamma_{sl} &= -2 \ln(\beta) \sqrt{\frac{mk_{sl}}{7(\pi^2 + \ln(\beta)^2)}} \end{aligned}$$

based on equations 30 and 43 from Deen and Kuipers [8]. The sliding friction depends on the tangential relative velocity \vec{v}_{ij}^t at the point of contact, which is given by

$$\vec{v}_{ij}^t = (\vec{v}_i - \vec{v}_j) - \vec{n}_{ij}(\vec{n}_{ij} \cdot (\vec{v}_i - \vec{v}_j)) + (a_i - \frac{\delta_{ij}}{2}) \vec{n}_{ij} \times \omega_i + (a_j - \frac{\delta_{ij}}{2}) \vec{n}_{ij} \times \omega_j.$$

The difference of the first two terms gives the part of the relative tangential velocity due to the movement of the center of mass, whereas the latter two terms give the part due to the rotation of the particles. The relative tangential velocity is then used to update the position of the spring used to model the sliding friction with

$$\vec{x}_{spring} = \vec{x}_{spring}^{old} + \vec{v}_{ij}^t \Delta t$$

where \vec{x}_{spring}^{old} refers to the position in the previous timestep. The force due to the sliding friction can then be determined from

$$\vec{F}_{ij}^{sl} = -k_{sl}\vec{x}_{spring} - \gamma_{sl}\vec{v}_{ij}^t. \quad (10)$$

Forces due to friction have a maximum value. If $\vec{F}_{ij}^{sl} > \mu_{sl}|\vec{F}_N|$ then set $\vec{F}_{ij}^{sl} = \mu_{sl}|\vec{F}_N|$, otherwise keep it as is.

Similar to the force due to sliding friction, the torque due to the rolling friction is given according to

$$\vec{F}_{ij} = -k_{ro}\vec{x}_{spring} - \gamma_{ro}\vec{v}_{ij}^t \quad (11)$$

$$\vec{\tau}_{ij} = \gamma_{ro}(\vec{n}_{ij} \times \vec{F}_{ij}) \quad (12)$$

where the rolling stiffness and dissipation are given by

$$k_{ro} = \frac{2}{5}k \quad (13)$$

$$\gamma_{ro} = \frac{2}{5}\gamma. \quad (14)$$

Once again, if $\vec{F}_{ij} > \mu_{ro}|\vec{F}_N|$ then set $\vec{F}_{ij} = \mu_{ro}|\vec{F}_N|$, otherwise keep it as is.

A.1 Range of drop heights

This section contains the calculations done to determine the kinetic energy range.

TABLE 2: The values of the variables used in SI-units.

| | | |
|------------------------|---------------|------------|
| gravity | $ g $ | 9.81 |
| density of rock | ρ_{rock} | 2500 [4] |
| volume baseball | V_{ball} | 0.0002 [7] |
| displacement ball | h_{ball} | 1 |
| displacement tree | h_{tree} | 10 |
| length tree | l_{tree} | 2 |
| radius tree | r_{tree} | 0.05 |
| density tree | ρ_{tree} | 500 [1] |
| radius glass particles | r_{glass} | 0.005 |

The kinetic energies of the ball and tree upon impact were calculated with $m_{ball}|g|h_{ball}$ and $m_{tree}|g|h_{tree}$ respectively. The mass of the baseball sized rock was determined from $m_{ball} = \rho_{rock}V_{ball} = 0.500kg$, which gives a kinetic energy of $4.91J$. The mass of the tree was determined similarly, but the volume of the tree needed to be approximated first. The tree was assumed to have a cylindrical trunk, with half the volume of the trunk as branches additionally. The density of the tree was based on the density of a pine tree, as those tend to grow at higher altitudes. This gave a mass of $m_{tree} = \rho_{tree}(1.5\pi r_{tree}^2 l_{tree}) = 11.78kg$, leading to an energy of $1.16 * 10^3 J$.

B Topography

This section contains the maximum kinetic energy vs drop height plots for slopes B, C and D briefly mentioned in section 3.2.2. In these plots it can be seen that the measured

maximum kinetic energy for avalanches increases with the drop height for lower angles. This increase no longer occurs once an angle is reached where most of the drop heights cause an avalanche. The cause for this is twofold. Firstly, moving avalanches act like a liquid, meaning that the particles flow per layer. The simulations in this paper have 2.5 layers of moveable particles. For the higher angles, the majority of the particles in the top 1.5 layers is already part of the avalanche, while the bottom layer stays still. This results in a very limited number of particles that can still change from lying still to becoming part of the avalanche, leading to a limit in how much the kinetic energy of the system can increase due to this. Secondly, the triggered avalanches are not violent enough for the existence of a gaseous layer. The particles in a gaseous layer would have far higher kinetic energies than those in the flowing layer of the avalanche, thus adding to the kinetic energy of the system without requiring more particles. Since the avalanches are not violent enough, this does not happen either, leading to a limit in the maximum kinetic energy of the triggered avalanches.

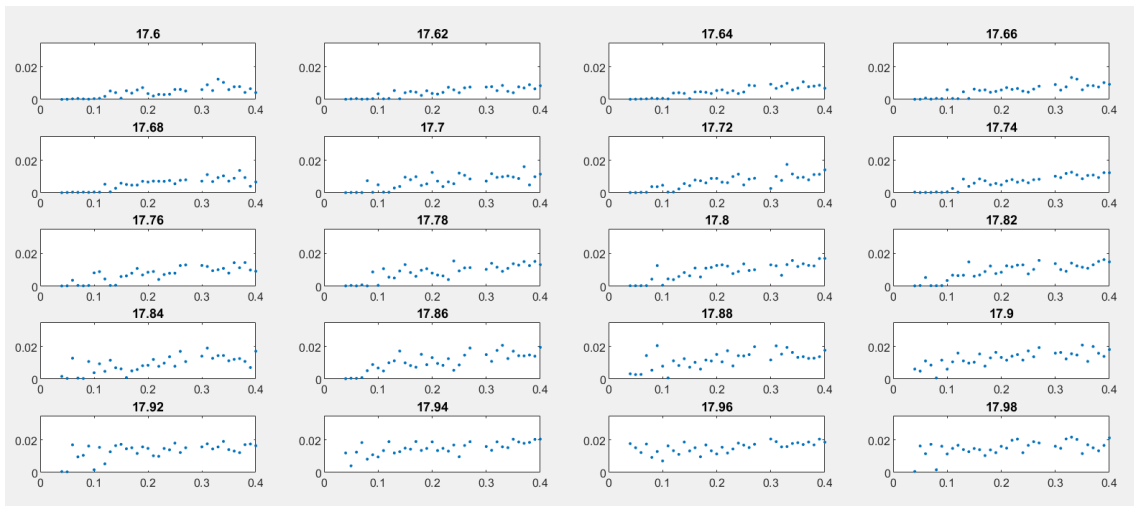


FIGURE 16: The triggered avalanches for slope B. Each subplot shows the maximum kinetic energy (J) per drop height (m) for a given slope angle ($^{\circ}$).

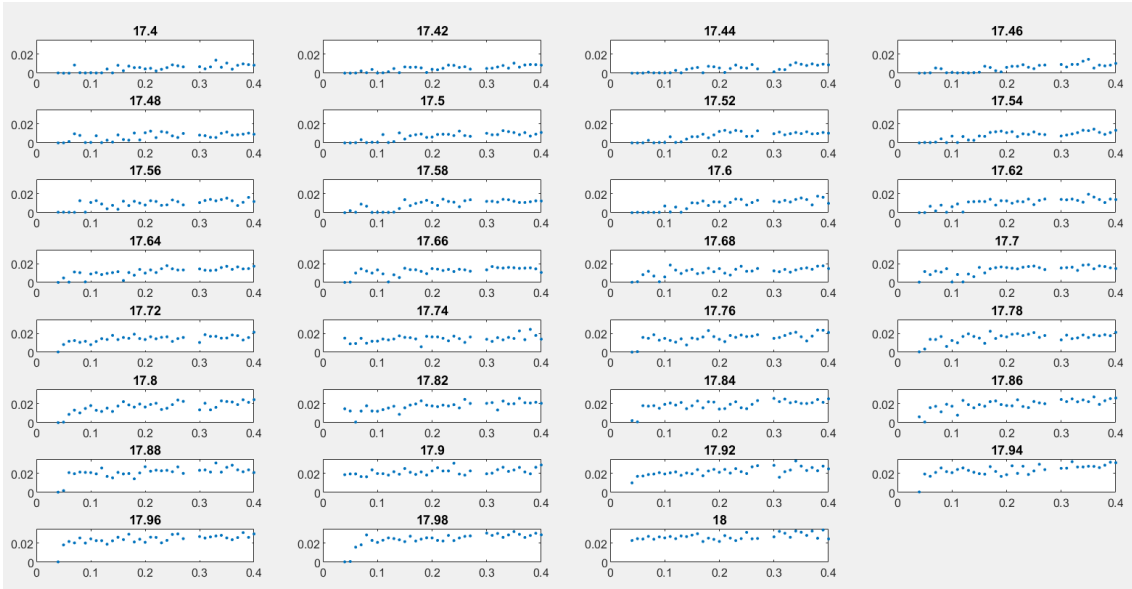


FIGURE 17: The triggered avalanches for slope C. Each subplot shows the maximum kinetic energy (J) per drop height (m) for a given slope angle ($^{\circ}$).

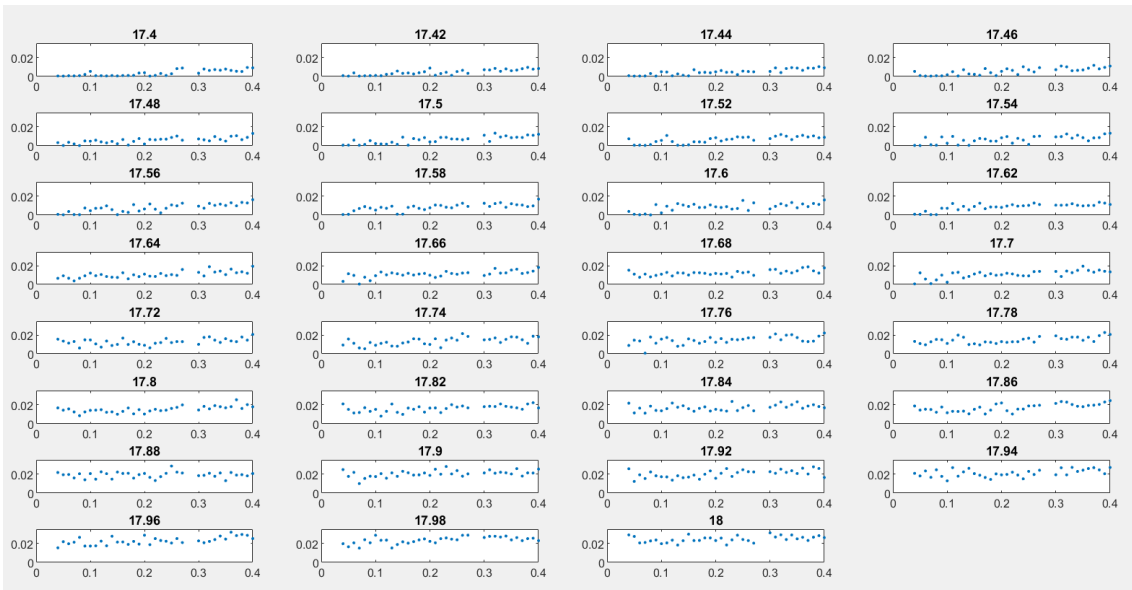


FIGURE 18: The triggered avalanches for slope D. Each subplot shows the maximum kinetic energy (J) per drop height (m) for a given slope angle ($^{\circ}$).

B.1 Slope E

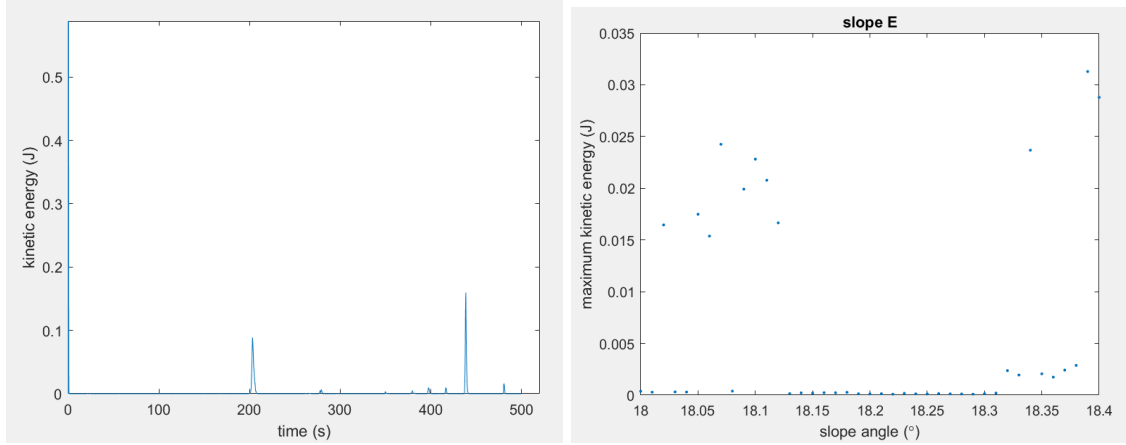


FIGURE 19: **left:** the kinetic energy (J) plotted against time (s) for slope E. **right:** the maximum kinetic energy (J) per slope angle ($^{\circ}$) obtained by running *findAngleofRepose*.

The expected angle of repose based on the left subplot is around 18.84° . There were no peaks in the kinetic energy before there, so on top of that this angle of repose deviates greatly from those of slopes A, B, C and D, there should not have been any kinetic energies above $0.008J$ in the right subplot. Since there are higher energies with no possible cause known to the author, no data from this slope was used in this paper.

C Additional figures

The mirrored plots show that the results on the left and right side of the slope have been mirrored as well. This indicates that there was no mistake in the code used for the simulations. The results are not perfectly mirrored due to the local topological influence.

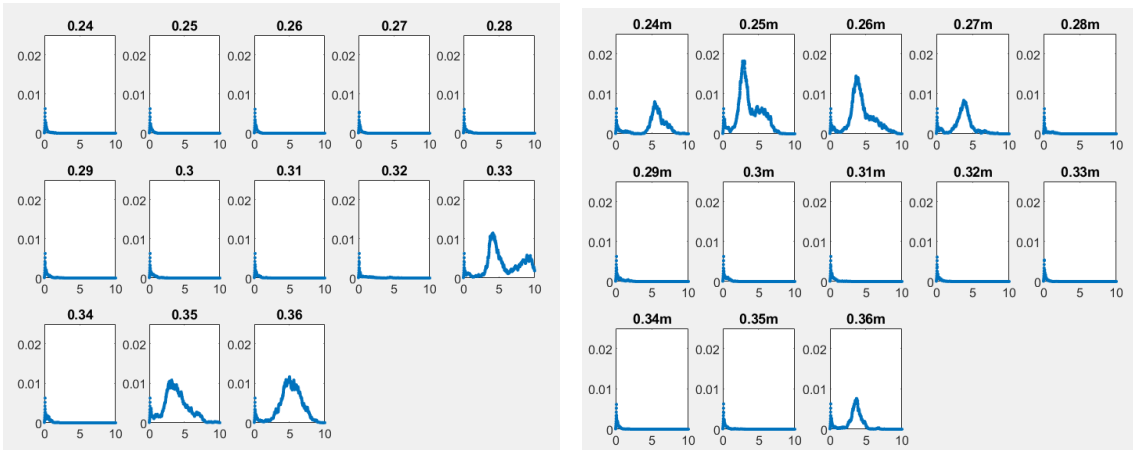


FIGURE 20: **left:** Each subplot shows the kinetic energy (J) of the system over time (s) for a given y-position in meters where the particle was dropped for $\alpha = 17.91^{\circ}$. **right:** The slope was mirrored over $y = 0.30m$. Each subplot shows the kinetic energy (J) of the system over time (s) for a given y-position in meters where the particle was dropped for $\alpha = 17.91^{\circ}$.